# Yrast structures of $^{98}$Nb and $^{99}$Mo

N. Fotiades,[1*] J. A. Cizewski,[2] P. Fallon,[3] P. G. Kevrekidis,[4] R. Krücken,[3] and I. Y. Lee[3]

[1]*Los Alamos National Laboratory, Los Alamos, New Mexico 87545, USA*

[2]*Department of Physics and Astronomy, Rutgers University, New Brunswick, New Jersey 08903, USA*

[3]*Nuclear Science Division, Lawrence Berkeley National Laboratory, Berkeley, California 94720, USA and*

[4]*Department of Mathematics and Statistics, University of Massachusetts, Amherst, Massachusetts 01003-4515, USA*

(Dated: November 19, 2024)

* Contact author: fotia@lanl.gov

# Abstract

**Background:** Neutron-rich nuclei in the A $\sim$ 100 mass region are interesting due to a rapid shape transition, especially pronounced in the Zr isotopes, and more recently observed in Nb isotopes. $^{98}$Nb, with only one proton and one neutron outside the subshell closure nucleus of $^{96}$Zr, is amenable to shell model calculations.

**Purpose:** To further examine the rapid shape transition the yrast structure of $^{98}$Nb was established in this work. This was the only yrast structure missing from all immediate neighbors to $^{96}$Zr.

**Method:** The yrast structure of $^{98}$Nb was studied in the fission of the compound systems formed in three heavy-ion induced reactions, $^{24}$Mg (134.5 MeV) + $^{173}$Yb, $^{23}$Na (129 MeV) + $^{176}$Yb, and $^{18}$O (91 MeV) + $^{208}$Pb. Prompt $\gamma$-ray spectroscopy was accomplished using the Gammasphere array.

**Results:** Excitation energies up to 3 MeV were observed for the first time in $^{98}$Nb. The yrast structure above the previously known $(5)^+$ isomer was established. In the process of studying $^{98}$Nb the yrast structure of positive-parity states in $^{99}$Mo was extended to 3.7 MeV excitation energy, the previously-known $^{99}$Nb level scheme was enriched, and two new levels were added in the level scheme of $^{97}$Zr.

**Conclusions:** The coupling of the odd proton occupying the $g_{9/2}$ orbital to the yrast states in the core nucleus of $^{97}$Zr can account for all observed states in $^{98}$Nb. The yrast structure for the positive-parity states of $^{99}$Mo is compared to the deformed ground-state bands of the $^{101}$Ru isotone and of $^{98,100}$Mo.

## I. INTRODUCTION

The properties of nuclei with partially filled nucleonic shells tend to exhibit smooth changes as the proton and neutron numbers vary. However, for nuclei with a few valence particles with respect to the subshell closure nucleus of $^{96}Zr_{56}$ rapid changes are observed in their level structures with increasing nucleon number. Addition of only four neutrons introduces considerable deformation [1]. In this mass region the interactions between nucleons lead to diverse shapes [2], including quantum phase transitions that involve shape changes [3], and with possible identification of triple shape coexistence in $^{96}$Sr and $^{98}$Zr [4].

Generally, interesting phenomena arise with abrupt deviations from a smooth pattern. The addition of an extra proton in the neighboring-to-Zr neutron-rich Nb isotopes is likely to enhance this rapid change of level structures. Indeed, a substantial degree of $\beta$ softness was observed before and after $N = 60$ for the Nb isotopes in laser spectroscopy [5].

The onset of deformation in the region of the nuclear chart around $Z = 40$ and $N = 60$ is attributed to depletion of protons from the orbitals of the $N = 3$ oscillator shell, accompanied by the occupation of proton $g_{9/2}$ orbitals, the filling of neutron $h_{11/2}$ orbitals, and the depletion of neutrons in the $g_{9/2}$ orbitals [6]. Specifically for the $N = 57$ isotones in the immediate vicinity of $^{96}$Zr a deformed structure was reported in $^{96}$Y [7].

The $^{98}$Nb isotope has only one proton and one neutron more than $^{96}$Zr. The $1^+$ spin-parity of the $^{98}$Nb ground state originates from the odd proton occupying the $g_{9/2}$ orbital and the odd neutron in the $g_{7/2}$ orbital with minimum-spin coupling. The first excited state, a 51.1 min isomer at 84(4)-keV excitation energy with a $(5)^+$ spin-parity assignment [8, 9], originates from the $\pi g_{9/2} \otimes \nu s_{1/2}$ maximally-aligned coupling. This isomer is the highest-spin state observed so far in $^{98}$Nb. The limited spectroscopic information that exists for $^{98}$Nb comes from a particle pick-up reaction and the $\beta$-decay of $^{98}$Zr [8, 9]. No $\gamma$ rays were known in $^{98}$Nb until recently, when eight $\gamma$ rays were assigned to $^{98}$Nb in a multinucleon-binary-grazing reaction experiment [10] without being possible to construct a level scheme out of these $\gamma$ rays. In the present work the construction of a $^{98}$Nb level scheme that includes two of these eight transitions was possible. On the other hand, in Ref. [10] an extensive level scheme for neighboring $^{99}$Nb was established and was only slightly enriched in the present work.

For nuclei in the immediate (plus or minus one proton and/or one neutron) vicinity of $^{96}$Zr

(i.e, $^{94,95,96}$Y [7, 11, 12], $^{95,97}$Zr [13–16], and $^{96,97,98}$Nb [10, 17]) medium-spin level schemes have been reported in all of them except in the heaviest among them, i.e., $^{98}$Nb. Moreover, $^{98}$Nb has the second lowest number of levels observed among the neighboring $N$=57 nuclei, as it is shown in Table I. Medium-spin states in $^{97}$Nb were established in Ref. [17] and were observed to follow closely the level pattern of $^{96}$Zr. The first medium-spin excited state in $^{97}$Nb (tentatively assigned as a $13/2^+$ state) was established at 1641.0 keV excitation energy, very close to the 1750.5 keV excitation energy of the first $2^+$ state in $^{96}$Zr. Furthermore, the similarity between the excitation energies of the $13/2^+$ states in the odd-mass Nb isotopes and the $2^+$ states in their corresponding even-mass Zr cores was pointed out in Ref. [17] for $N = 48$ to $N = 56$ and can be understood as originating from the coupling of the $g_{9/2}$ proton to the excitations in the core. The next link in this sequence is $^{98}$Nb with $N = 57$ neutrons, and in this picture it is especially interesting to compare the medium-spin level structure of $^{98}$Nb to the known one in the isotone $^{97}$Zr [15, 16].

In $^{99}$Mo a positive-parity yrast structure is built on the first excited state, a $5/2^+$, 15.5 $\mu$s isomer at 97.78-keV excitation energy, and was known up to ∼2.5 MeV excitation energy [24, 39]. The negative parity states become yrast above the previously known, $11/2^-$, 0.76 $\mu$s isomer at 684.1-keV excitation energy, with an $h_{11/2}$ decoupled-rotational band built on it [40]. In the process of studying $^{98}$Nb in the present work the positive-parity yrast structure of $^{99}$Mo was extended to 3.7 MeV excitation energy.

Prompt $\gamma$-ray spectroscopy of fission fragments has been proven to be an efficient way to study nuclei near the line of stability (see, for instance, Refs. [41, 42] and references therein). Such technique is complementary to studies based on Coulomb excitation and deep-inelastic processes, and helps bridge the gap in state systematics in areas between the neutron-deficient and neutron-rich nuclei, where dearth of experimental information is not uncommon. In the present work we used this technique to identify yrast structures in $^{98,99}$Nb and $^{99}$Mo.

## II. EXPERIMENTS

The 88-Inch Cyclotron Facility at Lawrence Berkeley National Laboratory was used to populate compound nuclei in three experiments henceforth referred to as Experiment I, II, and III. In all three experiments the emitted $\gamma$-rays were detected by the Gammasphere

array [43, 44]. In Experiment I, Gammasphere was comprised of 92 Compton-suppressed large volume HPGe detectors, while in Experiments II and III the number of Ge detectors was 100.

In Experiment I, a $^{197}$Pb compound nucleus (CN) was formed in the $^{24}$Mg + $^{173}$Yb reaction at 134.5 MeV. The target consisted of 1 mg/cm$^2$ isotopically enriched $^{173}$Yb, evaporated on a 7 mg/cm$^2$ gold backing (reactions of the beam in the backing produce a $^{221}$Pa CN). In Experiment II a $^{199}$Tl CN was formed in the $^{23}$Na + $^{176}$Yb reaction at a beam energy of 129 MeV. The target consisted of approximately 1 mg/cm$^2$ isotopically enriched $^{176}$Yb on a 10 mg/cm$^2$ Au backing (reactions of the beam in the backing produce a $^{220}$Th CN). In Experiment III a $^{226}$Th compound nucleus was populated in the $^{18}$O + $^{208}$Pb reaction at 91 MeV and the target was 45 mg/cm$^2$ in areal density.

With a width of the time overlap allowed between coincidences in the data acquisition trigger being $\sim$100 $ns$, a total of "prompt"-time 2.3$\times$10$^9$ triples, 10$^9$ quadrupels, and 2.5$\times$10$^9$ quadruples coincidence events were collected in Experiments I, II, and III, respectively. Symmetrized, three-dimensional cubes were constructed in all cases to investigate the coincidence relationships between the $\gamma$ rays. The analyses were performed with the RADWARE software package [45, 46].

## III. EXPERIMENTAL RESULTS

The level scheme of $^{98}$Nb deduced in the present work is shown in Fig. 1 and the information obtained for the transitions is summarized in Table II. This is the first observation of states with spin higher than five in this nucleus. The two lowest $\gamma$ rays (721.7- and 323.0-keV transitions) were first observed in a spectrum assigned to $^{98}$Nb in a multinucleon-binary-grazing reaction [10] without being possible to construct a level scheme. By placing gates in these two transitions in the experiments described above the other three $\gamma$ rays (851.8-, 917.6- and 988.0-keV transitions) were observed in all experiments and placed in the level scheme in Fig. 1. The three new transitions are not observed in the $^{98}$Nb spectrum in Ref. [10], supporting emission from higher spin states that are weakly populated in a multinucleon-binary-grazing reaction. The level scheme is now established up to $\sim$3 MeV excitation energy with the addition of five new levels.

The intensities of the 323-, and 988.0-keV transitions in Fig. 1, relative to the intensity

of the 721.7-keV transition, were obtained from a double gate on transitions of $^{93}$Nb [18] in Experiment I and were 42% and 78%, respectively. Similar relative intensities were observed in Experiment II. Moreover, the intensity of the 323-keV transition is quoted as 35% relative to that of the 722-keV transition in the multinucleon-binary-grazing reaction [10]. An isomeric half-life in the order of nanoseconds for the 1129-keV level in Fig. 1, similar to the 103-ns half-life of the 1264-keV level of $^{97}$Zr, can not be ruled out. In fact, the $\sim$100 $ns$ applied $\gamma$-$\gamma$ coincidence window mentioned in the previous section could help estimate the lifetime of such an isomer. Namely, assuming that there is no significant unobserved decay out of the 1129-keV level, and that the relative intensity from its sidefeeding is minimal, assumed here 6%, then a total of 84% relative intensity is feeding into the level (relative intensity of the 988.0-keV transition plus the sidefeeding). Only 42% (the intensity of the 323.0-keV transition) is observed to decay out of the 1129-keV level, i.e., only half of the intensity has decayed during the $\sim$100 $ns$ coincidence window. Hence, a $\sim$100 $ns$ half-life for the 1129-keV level is possible.

The level scheme of $^{99}$Mo deduced in the present work is shown in Fig. 2 and the information obtained for the transitions is summarized in Table II. The sequence built on the $5/2^+$, 15.5 $\mu$s isomer is now established up to $\sim$3.7 MeV excitation energy. The levels and transitions up to the $(17/2^+)$ state were previously known [24, 39], except for the 761.9-keV transition emitted from the previously known 2233-keV level. The tentative spin-parity assignments for the new levels is loosely based on the similar positive-parity sequence built on the ground state of the $^{101}$Ru [28] isotone, shown in Fig. 2. The intensity of the 137.5-, 600.5- and 807.8-keV transitions feeding directly the isomer are estimated from a spectrum gated on the 934.5- and 560.8-keV $^{92}$Zr [13] transitions, a complementary fragment to $^{99}$Mo, in Experiment I and are 62%, 40% and 38%, respectively, relative to the intensity of the previously known, 481.3-keV, $(15/2)^- \rightarrow 11/2^-$, transition emitted from the 1165.4 keV level of $^{99}$Mo [24] (not shown in Fig. 2). The latter was the strongest $^{99}$Mo transition observed in Experiment I.

The quality of the data obtained in Experiment I can be seen in the gated spectra on $^{98}$Nb transitions of Fig. 3. The presence of the transition from the $^{93}$Nb [18] complementary fragment to $^{98}$Nb, with accompanying emission of six neutrons, in both spectra further supports assignment of these transitions to $^{98}$Nb. Similar spectra, but with transitions from different complementary fragments, were obtained from Experiment II. The new transitions

assigned to $^{99}$Mo here (643.2- and 705.2-keV) can be seen in the sum of gated spectra shown in Fig. 4 together with the previously known transitions of the sequence built on the $5/2^+$, 15.5 $\mu$s isomer and transitions from the complementary fragments, $^{92,93}$Zr [13], with accompanying emission of six and five neutrons, respectively.

The partial level scheme for $^{99}$Nb established in the present work is shown in Fig. 5 and is consistent with that from the work of Kumar *et al.* [10] and the latest evaluation [24]. The information obtained for these transitions is summarized in Table III. Three new transitions were observed (105.4-, 243.5-, and 658.6-keV) and can be seen in the gates in Fig. 6. The 105.4-keV transition feeds into the previously known 765-keV level for which a $3/2^+$ spin-parity assignment was adopted in the latest evaluation [24]. In the upper spectrum in Fig. 6 the intensity of the 105.4-keV transition is three times less than the intensity of the 220.7-keV transition, after correcting for their relative detection efficiencies. From an intensity balance of the 765-keV level an internal conversion coefficient of $\sim$2 for the 105.4-keV transition could be possible. Thus, one would be tempted to assign an *M2* multipolarity to this transition. However, such an *M2* transition would compete unfavorably with the other transitions decaying out of the 870-keV level towards the lower $3/2^-$, $5/2^-$ and $(7/2^+)$ levels in Fig. 5. Hence, a $3/2^+$ spin-parity assignment for the 765-keV level might be incorrect, especially the positive-parity assignment, and, thus, the 765-keV level was included in the present work without a spin-parity assignment.

Last but not least, a partial level scheme for $^{97}$Zr established in the present work from Experiment III is shown in Fig. 7 together with gated spectra from Experiment III on these transitions. The information obtained for these transitions is summarized in Table IV. Two new transitions (730.5- and 855.0-keV) and two new levels (3448- and 4178-keV) were added above the previously-known $7/2^+$ level at 2593-keV excitation energy [16]. The latter is already an off-yrast state with the lowest $7/2^+$ level at 1264-keV excitation energy in Fig. 1, hence, both new levels are also, most likely, off-yrast states.

## IV. DISCUSSION

A comparison of the states established in $^{98}$Nb to known states in the yrast sequence of $^{97}$Zr [15] was included in Fig. 1. The energies and $\gamma$-ray decay patterns of the states in $^{98}$Nb suggest that a one-to-one correspondence can be made between the $^{98}$Nb and $^{97}$Zr yrast

excitations at least up to 3 MeV excitation energy, as seen in Fig. 1. Thus, the yrast states of $^{98}$Nb up to 3 MeV can be ascribed to the coupling of the odd proton occupying the $g_{9/2}$ orbital to the yrast states in the $^{97}$Zr core. The rapid change in the level structure with increasing nucleon number mentioned in Section I is illustrated in Fig. 1 by adding partial level schemes for $^{99}$Zr [24] and $^{100}$Nb [26].

Low-excited-state shell-model calculations in neighboring-to-$^{98}$Nb nuclei usually truncate the neutron valence space by keeping the $h_{11/2}$ orbit empty, with full occupation of the proton $2p_{3/2}$, $1f_{5/2}$, and $1f_{7/2}$ orbitals, and full occupation of the $1g_{9/2}$ neutron orbital (see, for instance, Ref. [10], and references therein). The excitation energy of an $11/2^-$ state, ascribed to the $\nu$h$_{11/2}$ orbital, in $^{97}$Zr remains experimentally elusive. For the 2264-keV level of $^{97}$Zr in Fig. 1 a $(11/2^-)$ spin-parity assignment was adopted in the latest evaluation [23] following suggestions in Refs. [15, 47] of a $\nu$h$_{11/2}$ single-particle configuration for this state. However, a $(9/2^+)$ spin-parity assignment was suggested in Ref. [16] for the same state. If the $\nu$h$_{11/2}$ single-particle interpretation for the 2264-keV level is correct then a $(10^-)$ spin-parity assignment can be suggested for the 2117-keV level of $^{98}$Nb. Subsequently, the $\nu$h$_{11/2}$ configuration in $^{97}$Zr and the $\nu$h$_{11/2} \otimes \pi$g$_{9/2}$ configuration in $^{98}$Nb would be at similar excitation energies, while in the $^{99}$Mo [24, 40] isotone, the $\nu$h$_{11/2}$ orbital drops further in excitation energy and becomes an isomer at 684.1-keV excitation energy with the yrast structure above it exhibiting characteristics of a rotational sequence. If the $(9/2^+)$ spin-parity assignment from Ref. [16] is correct, then a $(9^+)$ spin-parity assignment can be suggested for the 2117-keV level of $^{98}$Nb and the $\nu$h$_{11/2}$ configuration in $^{97}$Zr lies higher in excitation energy, as was discussed in Refs. [48, 49]. Furthermore, for the 1129-keV, $(8^+)$ state of $^{98}$Nb in Fig. 1, its configuration can be compared directly to the 1541-keV, $8^+$, 9.6 s spherical isomer known in the isotone $^{96}$Y [7], which is of the same nature, i.e., the $\nu$g$_{7/2} \otimes \pi$g$_{9/2}$ configuration, and the yrast states observed immmediately above it are of positive parity [7] with the strongest transition feeding into the isomer from the $(9^+)$, 2318-keV level [7]. The latter is at about the same excitation energy as the 2117-keV level of $^{98}$Nb in Fig. 1. For the 734-keV, $(8^-)$, 12.4 $\mu$s isomer of neighboring $^{100}$Nb [26] (also shown in Fig. 1), a possible $\nu$h$_{11/2} \otimes \pi$g$_{9/2}$ configuration was suggested from systematics in Ref. [50], however, theoretical calculations in Ref. [51] discuss the possibility for an $(8^+)$, $\nu$g$_{7/2} \otimes \pi$g$_{9/2}$ configuration which can not be ruled out for this state.

More experimental data are needed to determine the location of the $\nu$h$_{11/2}$ orbital in $^{97}$Zr

and $^{98}$Nb. If the 2264-keV state of $^{97}$Zr is not the $11/2^-$, $\nu h_{11/2}$ state, then the possibility that one of the new $^{97}$Zr states in Fig. 7 could be this state can not be ruled out. If the new 3448-keV state in Fig. 7 had a $9/2^+$ spin-parity assignment it would most likely get populated via the $\beta$-decay of the $(9/2)^+$, first-excited state of $^{97}$Y [23], which is an isomer. There are already several $9/2^+$ levels known in $^{97}$Zr with appreciable population in this $\beta$-decay and at about the same excitation energies [16]. Hence, a negative parity for the 3448-keV state is more likely if it has a $9/2$ $\hbar$ spin.

By addition of one more proton to the odd-odd $^{98}$Nb nucleus one produces the odd-mass $^{99}$Mo, a fission fragment that has been studied extensively because it is the $\beta$-decay parent nucleus of the $^{99m}$Tc radioisotope [24]. The latter is the most frequently used radioisotope in nuclear medicine for medical-imaging procedures and is also used for determining the number of fissions produced in the irradiation of uranium and plutonium by thermal neutrons [24, 52]. As a result, the total number of levels observed in Table I for $^{99}$Mo is much higher compared to that of $^{98}$Nb, which has the second lowest number. For $^{99}$Mo the positive-parity yrast states in Fig. 2 are built on the neutron $d_{5/2}$ orbital and appear similar to the ground-state band of the isotone $^{101}$Ru [40] where the $5/2^+$ ground state originates from the odd neutron occuping the same orbital. However, the structure in $^{101}$Ru is a well-formed rotational band that even exhibits a backbend at higher rotational frequencies. On the contrary, the $^{99}$Mo positive-parity states appear more vibrational-like, on a transition path from the subshell closure in $^{96}$Zr to a deformed $^{101}$Ru. They appear similar to the vibrational structure built on the $5/2^+$ ground state of the $^{105}$Cd [53] isotone, with the latter approaching the $Z$=50 shell closure, and similar to the octupole collectivity observed in neighboring $^{98}$Mo [54] (see Fig. 8). Nevertheless, as mentioned above, the yrast structure above the $\nu h_{11/2}$ orbital in $^{99}$Mo exhibits already characteristics of a rotational sequence, rendering $^{99}$Mo a transitional nucleus where both aspects coexist.

By addition of one more neutron to the odd-odd $^{98}$Nb nucleus one produces the odd-mass $^{99}$Nb, the fission fragment construed as the grandparent nucleus of the $^{99m}$Tc radioisotope discussed in the previous paragraph. The decay sequence of $^{99}$Nb in Fig. 5, starting with the 631-keV level and higher, was assigned Nilsson quantum numbers $5/2^-[303]$ in Ref. [10] based on comparison to the corresponding sequences in $^{101}$Nb [55] and $^{103}$Nb [56–58]. The $5/2^-[303]$ numbers were first assigned to one of these bands in Ref. [56] for the $^{103}$Nb sequence, where $g$-factors deduced experimentally for the $(9/2^-)$ and $(11/2^-)$ states match the theoretically-

predicted ones. Namely, experimental and theoretical values of the $|(g_K - g_R)/Q_0|$ ratio were reported as 0.04 $(e \bullet b)^{-1}$, [56] where $g_K$ is the factor for the intrinsic motion, $g_R = Z/A$ is the collective $g$-factor, and $Q_0$ is the quadrupole moment. Using the same formalism as in Ref. [56], and the branching ratios for the $(9/2^-)$ and $(11/2^-)$ states in Fig. 5 the experimental ratio increases to 0.13 $(e \bullet b)^{-1}$ in $^{99}$Nb, while the theoretical value also increases to 0.09 $(e \bullet b)^{-1}$. Hence, this negative-parity sequence in $^{99}$Nb might not be as purely collective as the corresponding one in $^{103}$Nb, at least at its lower part, as one would expect from the proximity of $^{99}$Nb to the subshell closure in $^{96}$Zr and the sudden onset of deformation at $N = 60$ [5].

With the addition of five new levels to $^{98}$Nb in the present work the total number of its excited states in Table I is increased by 30%. On the other hand, addition of two levels to $^{99}$Mo looks "negligible" compared to its previously-known number of levels in Table I. In fact, the total number of levels observed in Table I for $^{99}$Mo is the highest among all neighboring $N$=57 isotopes, and it is still ten times more than the known levels of $^{98}$Nb including those in the present work. Since $^{98}$Nb is an odd-odd nucleus a higher level fragmentation is expected compared to $^{99}$Mo, however, it is this increased fragmentation that hinders observation of these levels. This "staggering" in the observed number of levels between odd-odd and odd-mass nuclei is seen clearly in Table I, except as one approaches the $Z$=50 shell closure, where a gradual decrease is observed. The increased density of levels for $^{99}$Mo and $^{101}$Ru in Table I is also observed in the neighboring $N$=56 isotopes, as was reported in Ref. [59]. The maximum of the observed level density occurs between 2- and 3-MeV excitation energy as can be deduced from Fig. 9.

## V. SUMMARY

In summary, medium-spin states were observed for the first time in $^{98}$Nb following the fission of hot compound nuclei formed in three fusion-evaporation reactions. The assignment of the transitions is based on coincidences with previously known transitions in the complementary fragments and the recent observation of two of these transitions in a multinucleon-binary-grazing reaction experiment. Excited states in $^{98}$Nb up to 3 MeV can be interpreted as the coupling of the odd proton occupying the $g_{9/2}$ orbital to positive and negative parity yrast states in a $^{97}$Zr core. For the latter, two new transitions and two new off-yrast states

were observed in the present work. The spectroscopy of medium-spin states in the immediate vicinity of the subshell closure nucleus $^{96}$Zr is now complete and the gap at $A = 98$ in the systematics of medium-spin states in $N = 57$ isotones is now bridged.

The positive-parity structure above the $d_{5/2}$ odd-neutron isomer in $^{99}$Mo was extended to 3.7 MeV excitation energy and compared to that in the $^{101}$Ru isotone and the ground-state band of the $^{98}$Mo core. More experimental information, especially firm spin and parity assignments of the states reported here, is needed to confirm the interpretations, and new shell model calculations for nuclei near $^{96}$Zr are needed to compare with the medium-spin states observed in the present work.

**Acknowledgments**

The authors thank all the staff of Gammasphere at LBNL, with special thanks going to Augusto O. Macchiavelli. This work has been supported in part by the U.S. Department of Energy under Contract Nos. 89233218CNA000001 (LANL), DE-AC02-05CH1123 (LBNL), and by the National Science Foundation (Rutgers).

---

[1] E. Cheifetz, R. C. Jared, S. G. Thompson, and J. B. Wilhelmy, Phys. Rev. Lett. **25**, 38 (1970).

[2] K. Heyde and J. L. Wood, Rev. Mod. Phys. **83**, 1467 (2011).

[3] P. Cejnar, J. Jolie, and R. F. Casten, Rev. Mod. Phys. **82**, 2155 (2010).

[4] A. Petrovici, Phys. Rev. C **85**, 034337 (2012).

[5] B. Cheal, K. Baczynska, J. Billowes, P. Campbell, F. C. Charlwood, T. Eronen, *et al.*, Phys. Rev. Lett. **102**, 222501 (2009).

[6] A. Kumar and M. R. Gunye, Phys. Rev. C **32**, 2116 (1985).

[7] Ł. W. Iskra, *et al.*, Phys. Rev. C **102**, 054324 (2020).

[8] L. R. Medsker and H. T. Fortune, Phys. Lett. **58B**, 297 (1975).

[9] J. Chen and B. Singh, Nucl. Data Sheets **164**, 1 (2020).

[10] V. Kumar, *et al.*, Phys. Rev. C **108**, 044313 (2023).

[11] Ł. W. Iskra, *et al.*, Phys. Scr. **92**, 104001 (2017).

[12] W. Urban, *et al.*, Phys. Rev. C **79**, 044304 (2009).

[13] N. Fotiades, *et al.*, Phys. Rev. C **65**, 044303 (2002).

[14] D. Pantelica, *et al.*, Phys. Rev. C **72**, 024304 (2005).

[15] M. Matejska-Minda, *et al.*, Phys. Rev. C **80**, 017302 (2009).

[16] T. Rzaca-Urban, *et al.*, Phys. Rev. C **98**, 064315 (2018).

[17] N. Fotiades, J. A. Cizewski, R. Krücken, R. M. Clark, P. Fallon, I. Y. Lee, A. O. Macchiavelli, J. A. Becker, and W. Younes, Phys. Rev. C **82**, 044306 (2010).

[18] C. M. Baglin, Nucl. Data Sheets **112**, 1163 (2011).

[19] D. Abriola and A. A. Sonzogni, Nucl. Data Sheets **107**, 2423 (2006).

[20] I. Tsekhanovich, G. S. Simpson, W. Urban, J. A. Dare, J. Jolie, A. Linnemann, *et al.*, Phys. Rev. C **78**, 011301(R) (2008).

[21] S. K. Basu, G. Mukherjee, and A. A. Sonzogni, Nucl. Data Sheets **111**, 2555 (2010).

[22] D. Abriola and A. A. Sonzogni, Nucl. Data Sheets **109**, 2501 (2008).

[23] N. Nica, Nucl. Data Sheets **111**, 525 (2010).

[24] E. Browne and J. K. Tuli, Nucl. Data Sheets **145**, 25 (2017).

[25] S. J. Freeman, *et al.*, Phys. Rev. C **96**, 054325 (2017).

[26] B. Singh and J. Chen, Nucl. Data Sheets **172**, 1 (2021).

[27] J. Blachot, Nucl. Data Sheets **83**, 1 (1998).

[28] A. D. Yamamoto, *et al.*, Phys. Rev. C **66**, 024302 (2002).

[29] D. De Frenne, Nucl. Data Sheets **110**, 1745 (2009).

[30] D. Tonev, M. S. Yavahchova, N. Goutev, G. deAngelis, P. Petkov, R. K. Bhowmik, *et al.*, Phys. Rev. Lett. **112**, 052501 (2014).

[31] D. De Frenne, Nucl. Data Sheets **110**, 2081 (2009).

[32] J. Blachot, Nucl. Data Sheets **108**, 2035 (2007).

[33] Z. G. Wang, *et al.*, Phys. Rev. C **88**, 024306 (2013).

[34] S. Lalkovski, J. Timar, and Z. Elekes, Nucl. Data Sheets **161**, 1 (2019).

[35] D. De Frenne and A. Negret, Nucl. Data Sheets **109**, 943 (2008).

[36] A. Y. Deo, *et al.*, Phys. Rev. C **79**, 067304 (2009).

[37] A. Ekström, *et al.*, Eur. Phys. J. A **44**, 355 (2010).

[38] J. Blachot, Nucl. Data Sheets **109**, 1383 (2008).

[39] J. Dubuc, G. Kajrys, P. Lariviere, S. Pilotte, W. DelBianco, S. Monaro, Phys. Rev. C **37**, 954 (1988).

[40] P. H. Regan, *et al.*, Phys. Rev. C **68**, 044313 (2003).

[41] N. Fotiades, *et al.*, Phys. Rev. C **67**, 064304 (2003).

[42] N. Fotiades, *et al.*, Phys. Rev. C **84**, 054310 (2011).

[43] I. Y. Lee, Nucl. Phys. A 520, 641c (1990).

[44] R. V. F. Janssens and F. S. Stephens, Nucl. Phys. News **6**, 9 (1996).

[45] D. C. Radford, Nucl. Instrum. Methods Phys. Res., Sect. A **361**, 306 (1995).

[46] D. C. Radford, M. Cromaz, and C. J. Beyer, in *Proceedings of the Nuclear Structure 98 Conference*, Gatlinburg, 1998, edited by C. Baktash, AIP Conf. Proc. No. 481 (AIP, New York, 1999), pp. 570–580.

[47] G. Lhersonneau, P. Dendooven, S. Hankonen, A. Honkanen, M. Huhta, R. Julin, *et al.*, Phys. Rev. C **54**, 1117 (1996).

[48] E. T. Gregor, *et al.*, Eur. Phys. J. A **53**, 50 (2017).

[49] C. R. Bingham and G. T. Fabian, Phys. Rev. C **7**, 1509 (1973).

[50] J. Genevey, F. Ibrahim, J. A. Pinston, H. Faust, T. Friedrichs, M. Gross, and S. Oberstedt, Phys. Rev. C **59**, 82 (1999).

[51] G. Lhersonneau, S. Brant, and V. Paar, Phys. Rev. C **62**, 044304 (2000).

[52] S. Hasan and M. A. Prelas, SN Appl. Sci. 2, 1-28 (2020).

[53] D. Jerrestam, *et al.*, Nucl. Phys. **A593**, 162 (1995).

[54] S. Lalkovski, *et al.*, Phys. Rev. C **75**, 014314 (2007).

[55] Y. X. Luo, J. O. Rasmussen, I. Stefanescu, A. Gelberg, J. H. Hamilton, A. V. Ramayya, *et al.*, J. Phys. G: Nucl. Part. Phys. **31**, 1303 (2005).

[56] M. A. C. Hotchkis, J. L. Durell, J. B. Fitzgerald, A. S. Mowbray, W. R. Phillips, I. Ahmad, *et al.*, Nucl. Phys. **A530**, 111 (1991).

[57] M. Liang, H. Ohm, B. De Sutter, and K. Sistemich, Z. Phys. A **344**, 357 (1993).

[58] H. Hua, C. Y. Wu, D. Cline, A. B. Hayes, R. Teng, R. M. Clark, P. Fallon, A. O. Macchiavelli, and K. Vetter, Phys. Rev. C **65**, 064325 (2002).

[59] J. Wiśniewski, *et al.*, Phys. Rev. C **108**, 024302 (2023).

TABLE I: Total number of excited levels observed in the $N$=57 isotones from Kr to Sn and the corresponding references used.

| Proton Number | Number of levels | References |
|---|---|---|
| 36 | 12 | [18] |
| 37 | 29 | [19], [20] |
| 38 | 69 | [21] |
| 39 | 31 | [7], [22] |
| 40 | 68 | [15],[16],[23] |
| 41 | 16 | [9] |
| 42 | 216 | [24],[25] |
| 43 | 90 | [26] |
| 44 | 207 | [25],[27],[28] |
| 45 | 127 | [29],[30] |
| 46 | 114 | [31] |
| 47 | 96 | [32],[33] |
| 48 | 89 | [34] |
| 49 | 61 | [35],[36],[37] |
| 50 | 31 | [38] |

TABLE II: $\gamma$-ray energies (in keV), emitting-level excitation energies (in keV), prompt intensities, and emitting-level spin-parity assignments for transitions in $^{98}$Nb and $^{99}$Mo from Experiment I. Internal conversion corrections are not included in the quoted intensities. All quoted excitation energies for $^{98}$Nb inherit a 4-keV error from the previously quoted excitation energy of 84(4) keV [9] for the $(5)^+$ isomer in Fig. 1. The uncertainty on the $\gamma$-ray energies varies from 0.4 keV to 0.8 keV. The 323.0- and 721.7-keV transitions were first observed in a $\gamma$-ray spectrum assigned to $^{98}$Nb in Ref. [10]. The 851.8-, 917.6-, and 988.0-keV $^{98}$Nb transitions, as well as the 643.2-, 705.2-, and 761.9-keV $^{99}$Mo transitions were observed in the present work for the first time.

| $E_\gamma$ | $E_i$ | $I_\gamma$ | $J_i^\pi$ |
|---|---|---|---|
| | $^{98}$Nb | | |
| 323.0 | 1129(4) | 42(4) | $(8^+)$ |
| 721.7 | 806(4) | 100 | $(6^+)$ |
| 851.8 | 2968(4) | 23(3) | |
| 917.6 | 3034(4) | 16(3) | |
| 988.0 | 2117(4) | 78(5) | $(9^+, 10^-)$ |
| | $^{99}$Mo | | |
| 137.5 | 235 | 62(5) | $\frac{7}{2}^+$ |
| 207.5 | 906 | 14(3) | $(\frac{9}{2})^+$ |
| 462.8 | 698 | 8(2) | $(\frac{7}{2}^+)$ |
| 481.3 | 1165 | 100 | $(\frac{15}{2})^-$ |
| 565.2 | 1471 | 5(2) | $(\frac{11}{2}^+)$ |
| 600.5 | 698 | 40(4) | $(\frac{7}{2}^+)$ |
| 643.2 | 3051 | 13(3) | $(\frac{21}{2}^+)$ |
| 670.3 | 906 | 10(3) | $(\frac{9}{2})^+$ |
| 705.2 | 3757 | 8(2) | $(\frac{25}{2}^+)$ |
| 729.9 | 2408 | 20(3) | $(\frac{17}{2}^+)$ |
| 761.9 | 2233 | 8(2) | $(\frac{15}{2}^+)$ |
| 772.6 | 1678 | 30(4) | $(\frac{13}{2}^+)$ |
| 773.0 | 1471 | 14(3) | $(\frac{11}{2}^+)$ |
| 807.8 | 906 | 38(4) | $(\frac{9}{2})^+$ |

TABLE III: $\gamma$-ray energies (in keV), emitting-level excitation energies (in keV), prompt intensities, and emitting-level spin-parity assignments for transitions in $^{99}$Nb from Experiment II. Internal conversion corrections are not included in the quoted intensities. The uncertainty on the $\gamma$-ray energies varies from 0.4 keV to 0.8 keV. The 105.4-, 243.5-, and 658.6-keV transitions were observed in the present work for the first time.

| $E_\gamma$ | $E_i$ | $I_\gamma$ | $J_i^\pi$ |
|---|---|---|---|
| 87.0 | 631 | 30(5) | $\frac{5}{2}^-$ |
| 105.4 | 870 | 9(2) | $(\frac{7}{2}^-)$ |
| 178.6 | 544 | 100 | $\frac{3}{2}^-$ |
| 220.7 | 765 | 26(3) | |
| 238.8 | 870 | 60(5) | $(\frac{7}{2}^-)$ |
| 243.5 | 631 | 35(4) | $\frac{5}{2}^-$ |
| 250.7 | 1120 | 30(4) | $(\frac{9}{2}^-)$ |
| 282.0 | 1402 | 20(4) | $(\frac{11}{2}^-)$ |
| 314.1 | 1716 | 20(4) | $(\frac{13}{2}^-)$ |
| 325.6 | 870 | 9(3) | $(\frac{7}{2}^-)$ |
| 326.4 | 2043 | 5(2) | $(\frac{15}{2}^-)$ |
| 387.4 | 387 | 90(7) | $(\frac{7}{2}^+)$ |
| 482.5 | 870 | 25(3) | $(\frac{7}{2}^-)$ |
| 489.6 | 1120 | 40(4) | $(\frac{9}{2}^-)$ |
| 533.1 | 1402 | 46(5) | $(\frac{11}{2}^-)$ |
| 595.7 | 1716 | 42(4) | $(\frac{13}{2}^-)$ |
| 641.3 | 2043 | 20(3) | $(\frac{15}{2}^-)$ |
| 643.1 | 2359 | 30(4) | $(\frac{17}{2}^-)$ |
| 658.6 | 2702 | 14(3) | $(\frac{19}{2}^-)$ |

TABLE IV: $\gamma$-ray energies (in keV), emitting-level excitation energies (in keV), prompt intensities, and emitting-level spin-parity assignments for transitions in $^{97}$Zr from Experiment III. The uncertainty on the $\gamma$-ray energies varies from 0.4 keV to 0.8 keV. The 999.5-keV transition, which is the strongest $^{97}$Zr transition observed in Experiment III, is shown in Fig. 1. The 730.5- and 855.0-keV transitions were observed in the present work for the first time.

| $E_\gamma$ | $E_i$ | $I_\gamma$ | $J_i^\pi$ |
|---|---|---|---|
| 254.3 | 2593 | 3(1) | $\frac{7}{2}^+$ |
| 730.5 | 4178 | 5(2) | |
| 855.0 | 3448 | 13(3) | |
| 938.6 | 2339 | 12(3) | $\frac{7}{2}^+$ |
| 999.5 | 2264 | 100 | $(\frac{9}{2}^+, \frac{11}{2}^-)$ |
| 1193.0 | 2593 | 19(3) | $\frac{7}{2}^+$ |
| 1400.0 | 1400 | 66(6) | $\frac{5}{2}^+$ |

FIG. 1: Level scheme assigned to $^{98}$Nb in the present work. Transition and excitation energies are given in keV. The uncertainty on the $\gamma$-ray energies varies from 0.4 keV to 0.8 keV. The widths of the arrows of the transitions are representative of the intensity of the transitions in Experiment I. The information on the $(5)^+$, 84(4) keV, 51 min isomer was taken from Ref. [9]. The excitation energies of all $^{98}$Nb levels above it inherit its 4-keV error. Partial level schemes of $^{97}$Zr [15, 16], $^{99}$Zr [24], and $^{100}$Nb [26] are also included as an illustration of the rapid change in the level structure with increasing nucleon number.

FIG. 2: Partial level scheme of positive-parity states of $^{99}$Mo as observed in the present work. Transition and excitation energies are given in keV. The uncertainty on the $\gamma$-ray energies varies from 0.4 keV to 0.8 keV. The widths of the arrows of the transitions are representative of the intensity of the transitions in Experiment I relative to the intensity of the previously known, 481.3-keV, $(15/2)^- \rightarrow 11/2^-$, transition emitted from the 1165.4 keV level of $^{99}$Mo [24] (not shown in the figure). This was the strongest $^{99}$Mo transition observed in Experiment I. The white part of the 137.5-keV arrow is representative of the relative-intensity correction due to internal conversion assuming a stretched transition. The information on the $5/2^+$, 97.78 keV, 15.5 $\mu$s isomer is taken from Ref. [24]. A partial level scheme of $^{101}$Ru [28] is also included for comparison.

FIG. 3: Background subtracted spectra from the $^{197}$Pb(CN) Experiment I gated on pairs of transitions of $^{98}$Nb in Fig. 1. The energies of the transitions are in keV. The 949.81-keV, $13/2^+ \rightarrow 9/2^+$ transition associated with the complementary $^{93}$Nb [18] isotope is indicated. Unlabelled peaks in both spectra are most likely contaminants. For instance, the upper spectrum has noticeable contamination from a concurrent gate on the 320.3- and 722.9-keV transitions of $^{97}$Mo [23]. Specifically, the peak next to the 851.8-keV transition in the upper spectrum is the 846.4-keV, $(23/2^-) \rightarrow (19/2^-)$ transition of $^{97}$Mo, the 1116.88-keV, $9/2^+ \rightarrow 5/2^+$ transition of $^{97}$Mo is also unlabelled in the upper spectrum, and $\sim$50% of the counts under the $^{93}$Nb peak was estimated to originate from the 947.0-keV, $(27/2^-) \rightarrow (23/2^-)$ transition of $^{97}$Mo. On the other hand, the lower spectrum is practically uncontaminated.

FIG. 4: Sum of background subtracted spectra from Experiment I gated on all pairs of the 729.9-, 772.6-, and 807.7-keV transitions of $^{99}$Mo in Fig. 2. The energies of the transitions are in keV. The 934.5-keV, $2^+ \rightarrow 0^+$, and 949.8-keV, $(9/2^+) \rightarrow 5/2^+$, transitions associated with the complementary $^{92,93}$Zr [13] isotopes, respectively, are indicated. Unlabelled peaks are most likely contaminants. For instance, the peak at ∼850 keV is not observed in Experiment II, hence, it is deemed a contaminant, although its provenance remains ambiguous.

FIG. 5: Partial level scheme of $^{99}$Nb as observed in the present work. Transition and excitation energies are given in keV. The uncertainty on the $\gamma$-ray energies varies from 0.4 keV to 0.8 keV. The widths of the arrows of the transitions are representative of the intensity of the transitions in Experiment II. The white part of the arrows is representative of the relative-intensity correction due to internal conversion assuming stretched transitions. The information on the $1/2^-$, 365-keV, 2.5 min isomer is taken from Ref. [24].

FIG. 6: Background subtracted spectra from Experiment II gated on transitions of $^{99}$Nb in Fig. 5. The energies of the transitions are in keV. Unlabelled peaks are most likely contaminants. For instance, the 486-keV peak in the upper spectrum is a doublet between the 482.5- and 489.6-keV transitions in Fig. 5 and is present in the spectrum because $^{95}$Zr is a complementary fragment to $^{99}$Nb in Experiment II (with accompanying emission of five neutrons) and also the level scheme of $^{95}$Zr [21] has a 178.3-keV, $(25/2^+) \rightarrow (23/2^+)$ transition which forms part of the gate in the upper spectrum.

FIG. 7: Partial level scheme of $^{97}$Zr as observed in the present work. Transition and excitation energies are given in keV. The uncertainty on the $\gamma$-ray energies varies from 0.4 keV to 0.8 keV. The widths of the arrows of the transitions are representative of the intensity of the transitions in Experiment III, relative to the intensity of the previously known, 999.5-keV transition shown in Fig. 1, which was the strongest $^{97}$Zr transition observed in Experiment III. Spins and parities are taken from Ref. [16]. Background subtracted spectra from Experiment III gated on these transitions are also included. Unlabelled peaks in the spectra are most likely contaminants.

FIG. 8: Comparison of positive-parity states of $^{99}$Mo from Fig. 2 to the ground-state bands in neighboring $^{98,100}$Mo [54].

FIG. 9: Level density in bins of 200 keV of experimentally-established excited states in $N$=57 Mo [24, 25], Ru [25, 27, 28], and Pd [31] isotopes. The two new $^{99}$Mo levels from Fig. 2 were included.

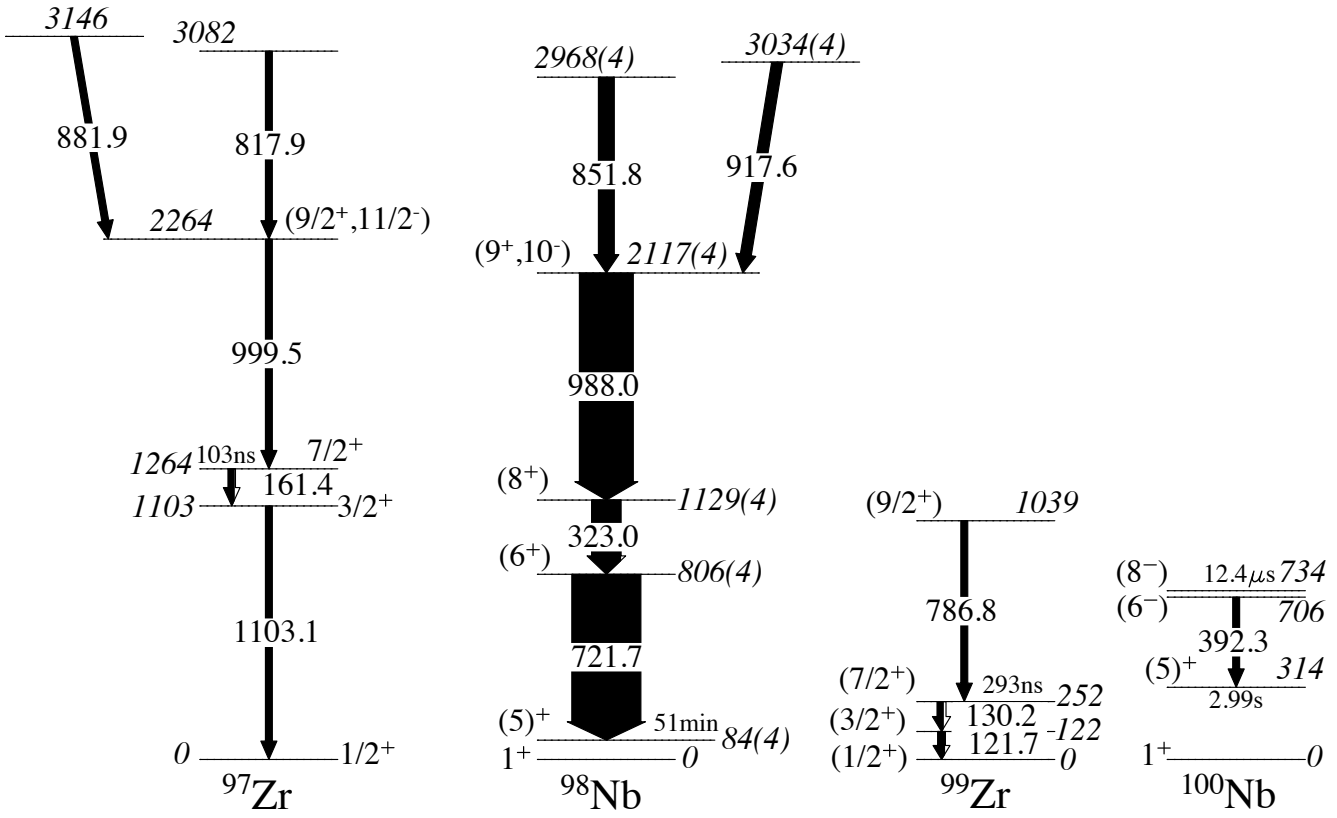


Fig 1
*N. Fotiades et al.*

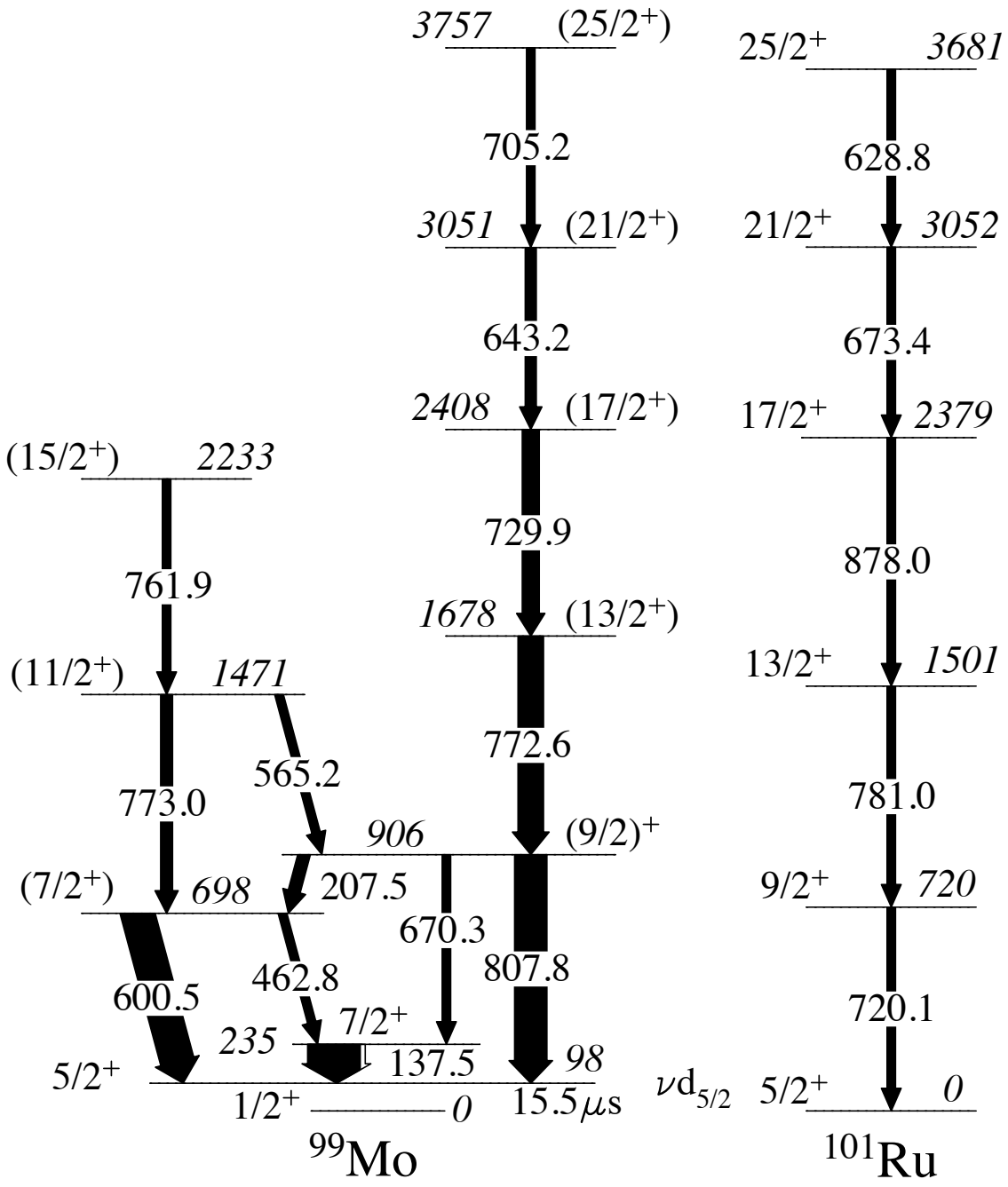


Fig 2
*N. Fotiades et al.*

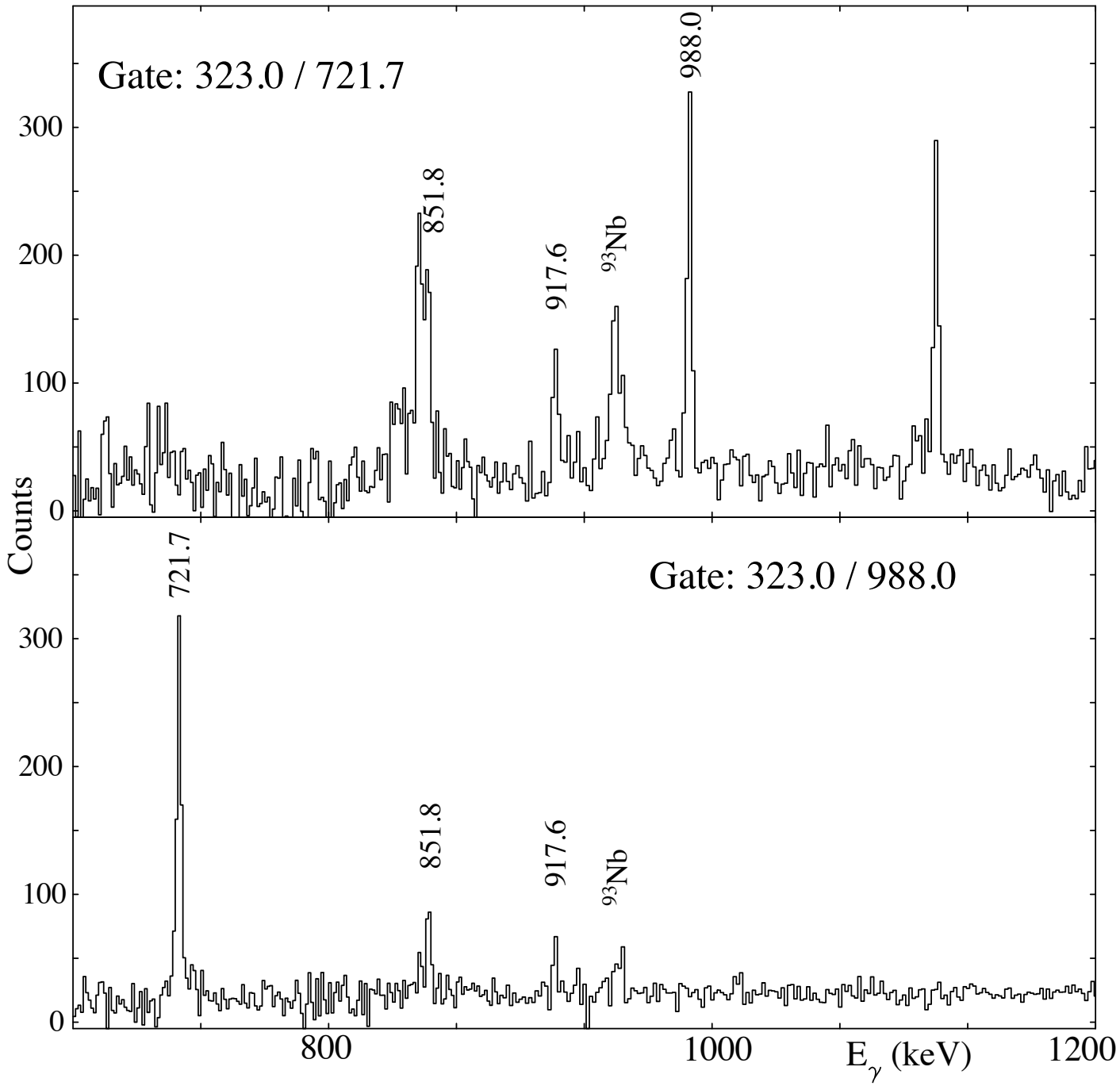


Fig 3
*N. Fotiades et al.*

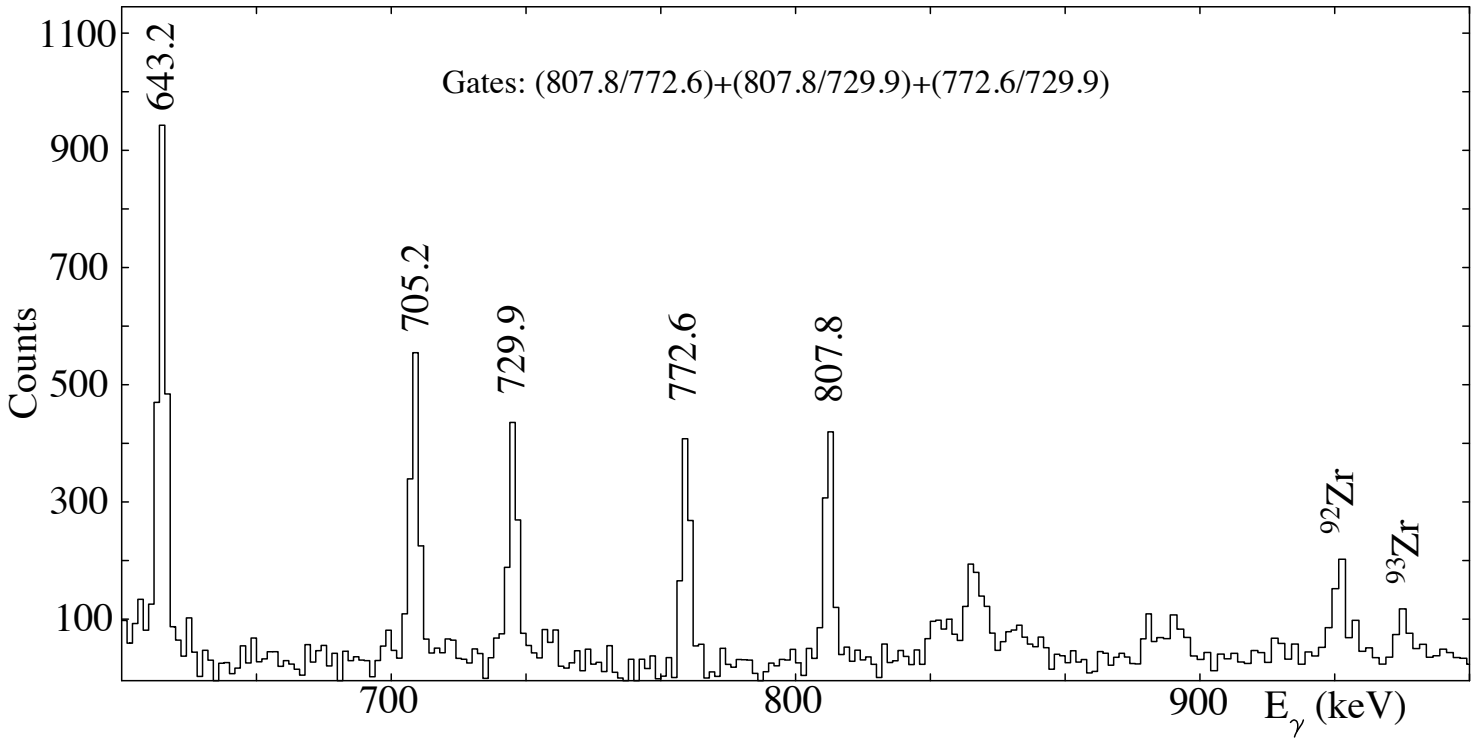


Fig 4

*N. Fotiades et al.*

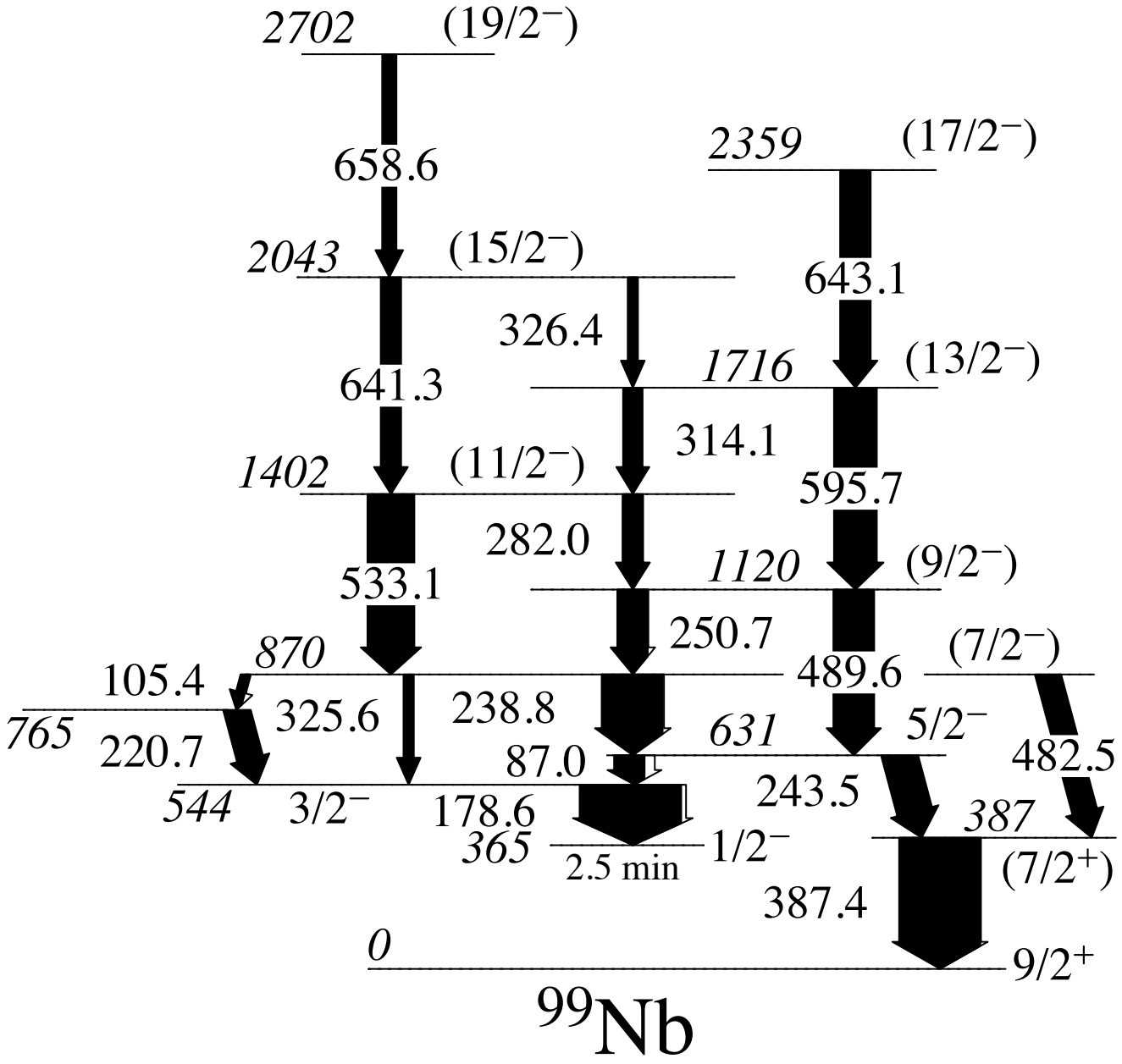


Fig 5
*N. Fotiades et al.*

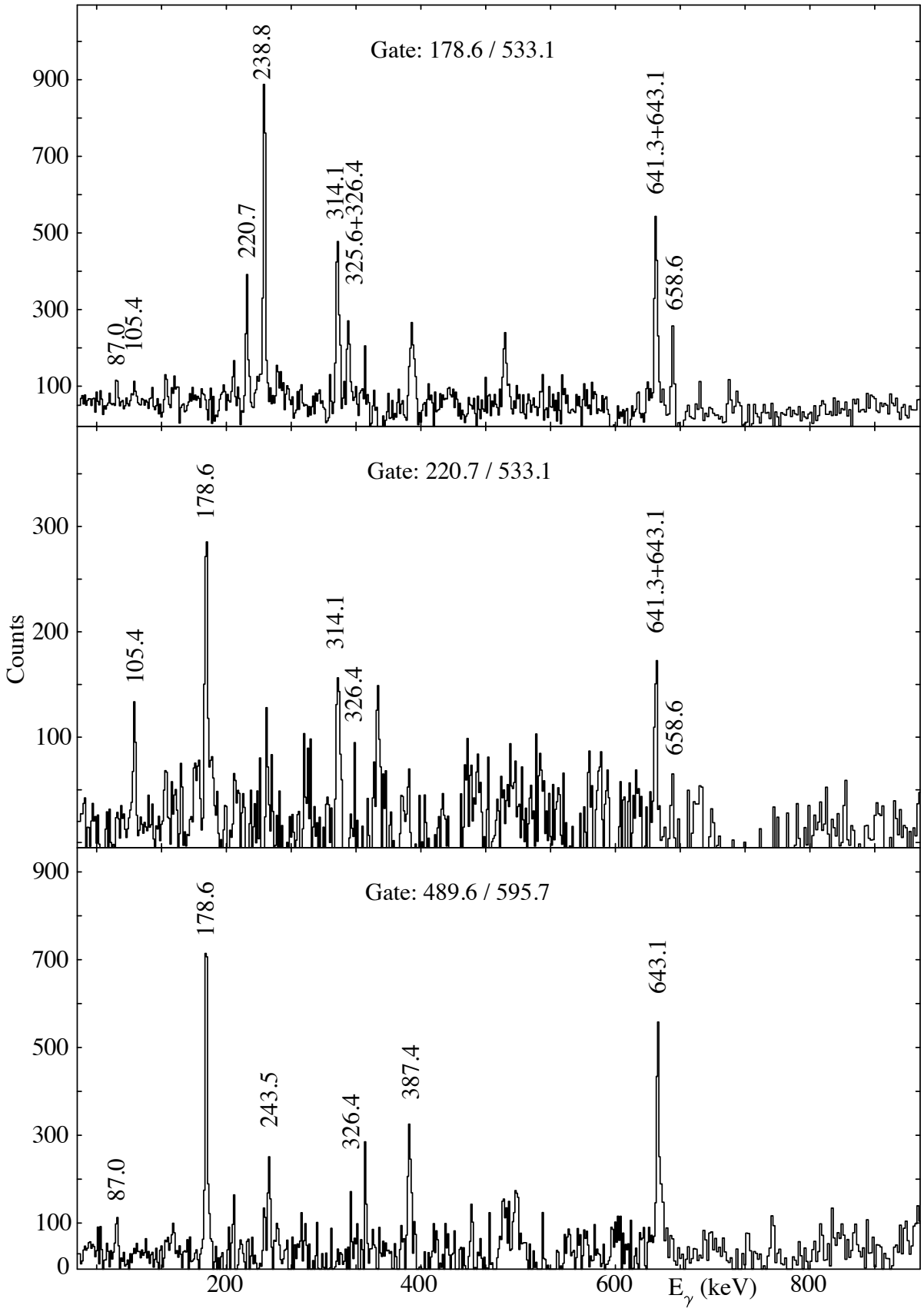


Fig 6
*N. Fotiades et al.*

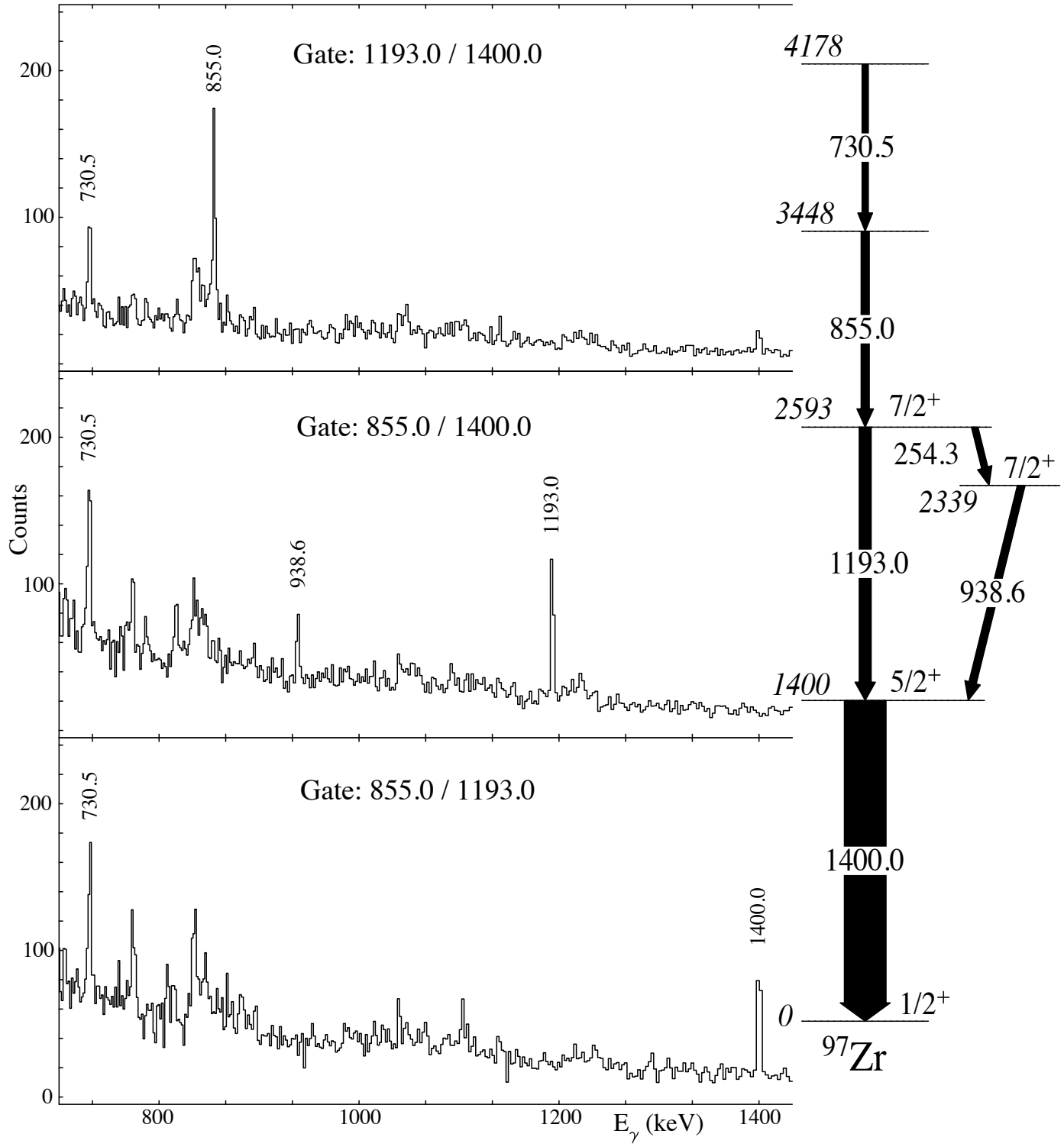


Fig 7
*N. Fotiades et al.*

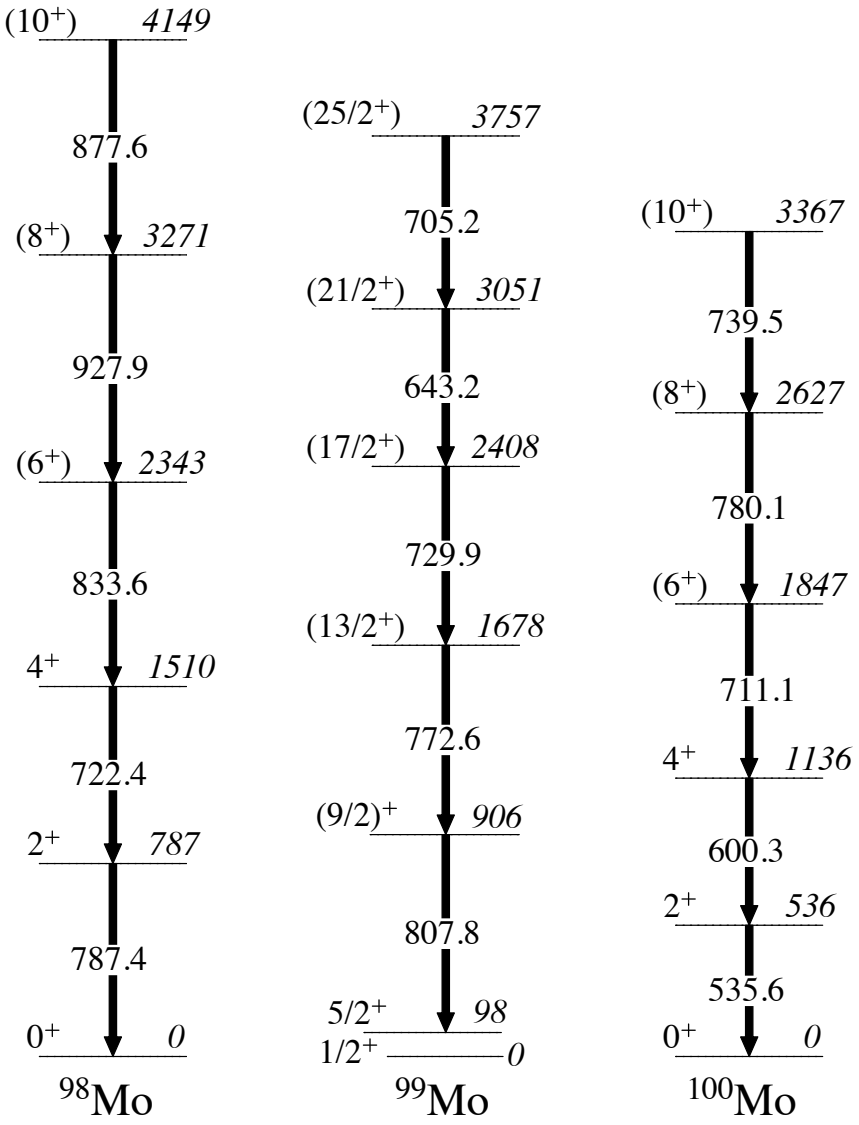


Fig 8
*N. Fotiades et al.*

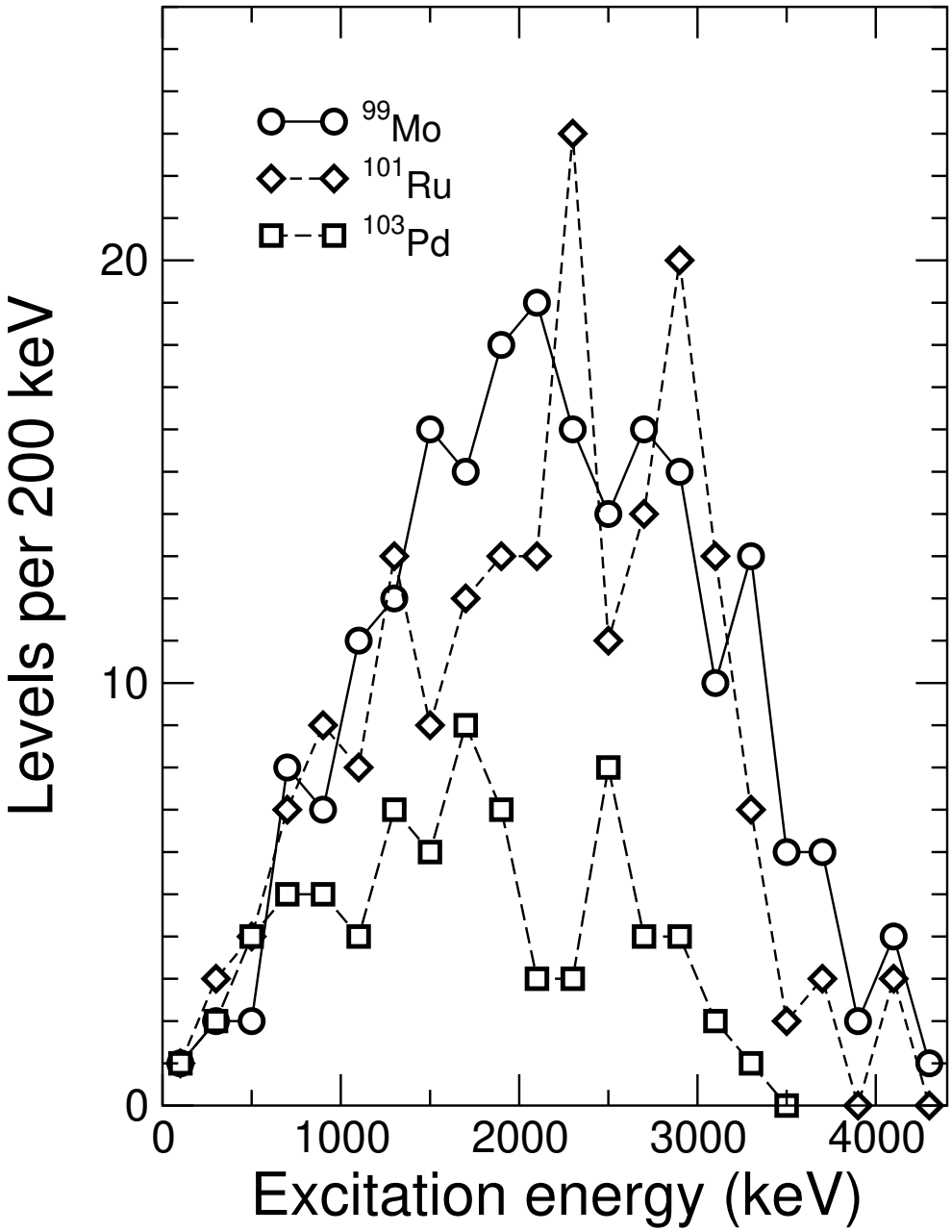


Fig 9

*N. Fotiades et al.*